

Anionic Effect on Enhancing the Stability of a Solid Electrolyte Interphase Film for Lithium Deposition on Graphite

Gaojing Yang, Simeng Zhang, Suting Weng, Xiaoyun Li, Xuefeng Wang,* Zhaoxiang Wang,* and Liqun Chen



Cite This: <https://doi.org/10.1021/acs.nanolett.1c01436>



Read Online

ACCESS |



Metrics & More



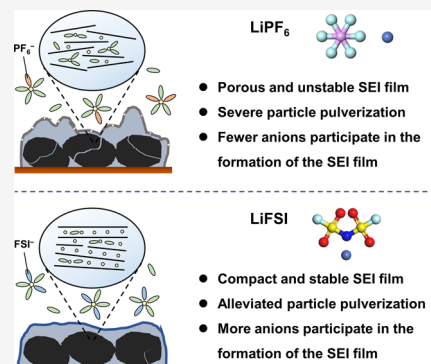
Article Recommendations



Supporting Information

ABSTRACT: Graphitic carbons and their lithium composites have been utilized as lithium deposition substrates to address issues such as the huge volume variation and dendritic growth of lithium. However, new problems have appeared, including the severe exfoliation of the graphite particles and the instability of the solid electrolyte interphase (SEI) film when metallic lithium is plated on the graphite. Herein, we enhance the stability of the SEI film on the graphite substrate for lithium deposition in an electrolyte of lithium bis(fluorosulfonyl)imide (LiFSI) dissolved in the carbonate solvent, thereby improving the lithium plating/stripping cycle on it. The FSI⁻ anion was found to be responsible for the formation of a compact SEI film under the lithium plating potential and could protect the graphite substrate. These findings refresh the understanding of the SEI stability and provide a suggestion on the design and development of electrolytes for the lithium batteries.

KEYWORDS: lithium deposition, graphite, LiFSI, solid electrolyte interphase (SEI), carbonate electrolyte



Issues such as a huge volume variation, an unstable solid electrolyte interphase (SEI) film, and the severe growth of lithium dendrites have to be well addressed before lithium-metal batteries can be commercialized.¹ Graphitic carbons^{2,3} and their lithium composites^{4,5} were recently utilized as lithium deposition substrates to solve the above problems. More recently, a lithium-ion/lithium-metal hybrid cell was proposed, in which graphite was used as the anode for both lithium intercalation and lithium plating to boost the energy density.⁶

Applications with graphite as a substrate for lithium plating is both attractive and challenging. Graphite has been extensively used as the host of the reversible lithium intercalation in ethylene carbonate (EC) electrolytes in Li-ion batteries (LIBs).⁷ Nevertheless, new challenges appear when metallic lithium is subsequently plated on it. It was reported that the chemical intercalation of the lithium ions in graphite can take place concurrently with lithium deposition.⁸ Our recent work showed that severe exfoliation occurs on commercial graphite during lithium plating due to the reductive decomposition of the SEI film.^{9,10} These indicate that structural degradation due to the co-intercalation of the solvated lithium ions is inevitable if the usual SEI film in the conventional electrolyte is destructed with the metallic lithium deposited on the graphite substrate. However, rare work has been conducted to alleviate the co-intercalation under the lithium plating potential.

The formation of a compact and stable SEI film is indeed an important prerequisite for maintaining the stability of the

graphite structure and the safety of lithium deposition. Unfortunately, disadvantages such as the chemical instability of the SEI film during lithium plating hamper the application of the carbonate electrolyte in lithium metal batteries.¹¹ Considering the importance of the carbonate electrolyte in practical secondary lithium batteries, many efforts have been made to improve the stability of the SEI films. Film-forming additives,^{12,13} multisalt electrolytes,^{14,15} and fluorinated electrolytes^{16,17} were developed to improve the interface stability and the cycling performance of the lithium metal anodes. These works demonstrate the necessity and feasibility of tuning the stability of the SEI film by optimizing the electrolyte composition.

Lithium salts have important impacts on the morphology of the deposited lithium and the Coulombic efficiency (CE) of the battery.¹⁸ Due to its high lithium-ion transference number¹⁹ and unique ability to form stable SEI films, lithium bis(fluorosulfonyl)imide (LiFSI) has been extensively studied as a popular salt for protecting the metallic lithium anodes.^{20–23} However, the case becomes much more complicated when metallic lithium is deposited on its graphite

Received: April 14, 2021

Revised: May 30, 2021

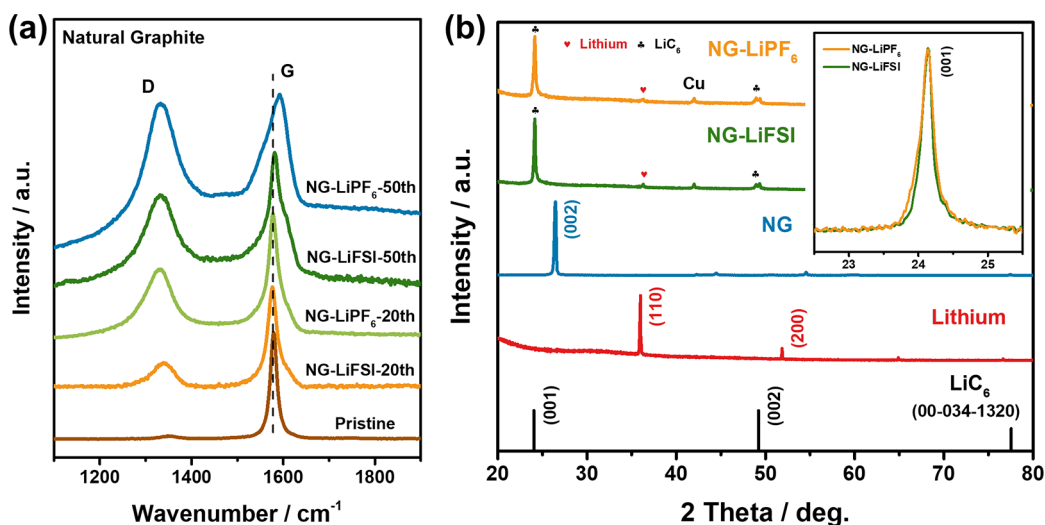


Figure 1. (a) The Raman spectra of the natural graphite after different lithium plating/stripping cycles and (b) the XRD patterns of the discharged natural graphite after 20 cycles in the two electrolytes (the “standard” XRD patterns for the metallic lithium and LiC_6 are shown for reference).

substrate. The SEI film has to be both stable on lithium and integral to the graphite that might otherwise be attacked with the deposited lithium. The metallic lithium destructs the SEI film on the graphite, leading to solvated lithium-ion co-intercalation, and the lithium becomes homeless. In this contribution, we enhance the stability of the SEI film on the graphite substrate using LiFSI. Both the protection of the graphite substrate and the improved lithium cycling performance on it indicate that the stability of the electrode/electrolyte interface is reinforced by the FSI^- -derived compact SEI film under the lithium plating potential. These findings reveal the important role of the FSI^- anion in constructing a compact and stable SEI film to protect the graphite and enhance the lithium cycling on it.

■ SUPPRESSED STRUCTURAL DEGRADATION OF GRAPHITE

The electrochemical performance of carbon materials is closely related to their structures. Our recent studies showed that severe exfoliation occurs for natural graphite during lithium plating in the LiPF_6 electrolyte (1 M LiPF_6 dissolved in EC and dimethyl carbonate (DMC) (1:1 v/v)).⁹ Replacing LiPF_6 with LiFSI in this work (the LiFSI electrolyte), the exfoliation of graphite is alleviated, as was verified with the difference in the intensity ratio of the D band compared to that of the G band (I_D/I_G) in the Raman spectra as well as the width of the (001) diffraction of the LiC_6 in the two electrolytes (Figure 1). The intensity ratio I_D/I_G increases more quickly in the LiPF_6 electrolyte than in the LiFSI electrolyte in the first 20 or more cycles (Figure 1a), and the broadening of the (001) diffraction in the LiPF_6 electrolyte is more obvious (Figure 1b). Furthermore, the structural destruction below 0.0 V in the LiPF_6 electrolyte also degrades the lithium-ion intercalation/deintercalation performances of the graphite in the subsequent cycles (Figure S1). These actually mean that the SEI film that is stable during lithium intercalation in graphite is severely damaged below 0.0 V in the LiPF_6 electrolyte and cannot protect the graphite from the Li^+ -solvent co-intercalation induced particle pulverization. In contrast, the SEI film formed in the LiFSI electrolyte can better protect the graphite below 0.0 V. In addition, obvious metallic lithium was detected on

the lithium-stripped graphite in the LiPF_6 electrolyte, while almost no metallic lithium was observable on the charged graphite in the LiFSI electrolyte (Figure S2).

■ ELECTROCHEMICAL EVALUATION

The electrochemical performances of the natural graphite (NG) using the LiFSI and LiPF_6 electrolytes are compared in Figure 2. For convenience, the cells using the LiFSI and LiPF_6 electrolytes are noted as the NG–LiFSI cell and the NG– LiPF_6 cell, respectively. The CE at a current density of 0.5 mA cm^{-2} is 32.8% and 34.5% for the NG–LiFSI cell and the NG– LiPF_6 cell in the first cycle, respectively, but sharply increases to 89.2% and 86.1% in the second cycle (Figure 2a). The low initial CE is attributed to the incomplete extraction of the intercalated lithium ions at the low cut-off charge potential (0.1 V vs. Li^+/Li ; Figure S3) as well as the irreversible reduction of the electrolyte below 0.8 V. The CE of the NG–LiFSI cell sharply rises to about 93.5% in a few cycles and remains stable for over 70 cycles. In contrast, the CE of the NG– LiPF_6 cell becomes unstable after the first few cycles and drops sharply after around 30 cycles. Even at temperatures up to 60°C , the cycling performance of the NG–LiFSI cell is still much better than that of the NG– LiPF_6 cell (Figure S4). In addition, LiFSI as an additive (0.1 M) in the LiPF_6 electrolyte can also improve the lithium cycling on graphite (Figure S5). These indicate that the cycling performance of the lithium deposited on graphite is better in the LiFSI electrolyte than in the LiPF_6 electrolyte.

At the early stage of lithium plating and the late stage of lithium stripping, the polarization is obviously lower; however, the nucleation overpotential remains the same in both electrolytes (Figure 2b). This means that the stability of the SEI film formed in the two electrolytes is different in the proceeding from lithium nucleation to the early lithium deposition. The cycling of lithium plating/stripping on the ball-milled graphite (BMG; the BMG–LiFSI cell) is even better in the LiFSI electrolyte (Figure S6) thanks to the suppressed particle pulverization of the BMG electrode (Figure S7).⁹

Figure 2c shows the lithium plating and stripping behaviors on graphite in the LiFSI electrolyte. The lithium plating and

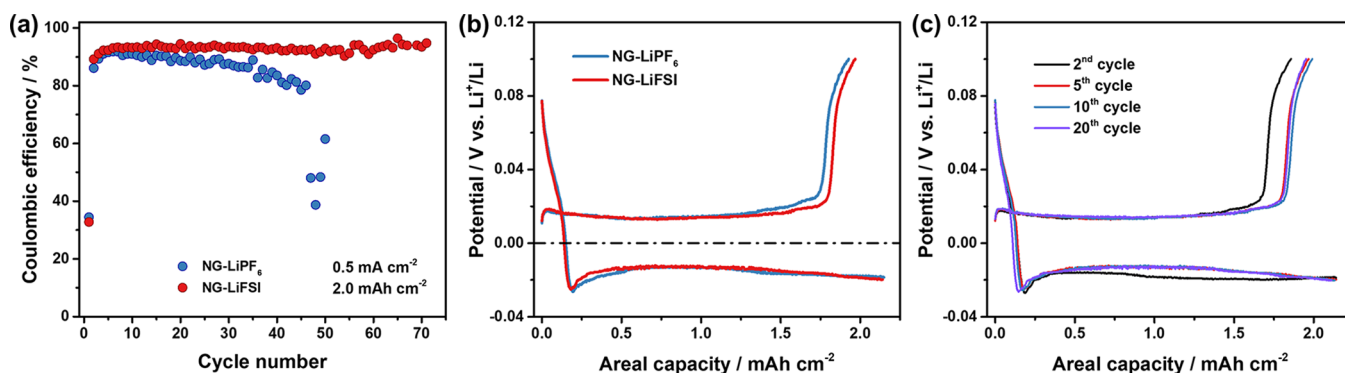


Figure 2. Comparison of (a) the Coulombic efficiencies, (b) the lithium plating and stripping potential profiles of the fifth cycle in different electrolytes, and (c) some selected potential profiles of the NG-LiFSI cell, all of which were recorded at a current density of 0.5 mA cm^{-2} for a lithium plating capacity of 2.0 mA h cm^{-2} .

stripping potentials remain stable after the first cycle, and the cell can stably run for over 550 h (Figure S8). In contrast, the polarization of the NG-LiPF₆ cell gradually increases, and the cell can only work for less than 350 h.

The impedance spectra (Figure S9) show that the SEI resistance (R_{SEI}) and charge transfer resistance (R_{CT}) of the NG-LiFSI cell are lower than those of the NG-LiPF₆ cell. Moreover, the deposited lithium is loose and dendritic in the LiPF₆ electrolyte but large and compact in the LiFSI electrolyte (Figure S10). Furthermore, the lithium particles on the ball-milled graphite (BMG) are larger and more compact (Figure S10), and the interface impedance of the BMG-LiFSI cell is lower than that of the NG-LiFSI cell (Figure S9).

■ COMPARISON OF PROTECTIVE INTERPHASE FILMS

The formation and properties of the SEI film are highly dependent on the chemical composition of the electrolyte. Fourier-transformed infrared spectroscopy (FTIR, Figure S11), X-ray photoelectron spectroscopy (XPS, Figure 3a–e), and cryogenic transmission electron microscopy (cryo-TEM, Figure 3f–h) were carried out to recognize the composition and structure of the SEI film on the discharged graphite after 20 cycles. The FTIR spectra show that organics (ROCOOLi and ROLi)²⁴ are the dominating components in both electrolytes, and some inorganic species (Li₂CO₃, LiF and Li₂O) can also be observed (Figure S11).

The XPS results confirm that organics are the dominating species of the SEI films in both electrolytes (Figure 3), agreeing with the FTIR spectroscopy results. The organic component is beneficial for enhancing the flexibility of the SEI films.²⁵ They may also play an important role in the lithium-ion transport in the interphase. The depth analysis shows that the content of the C–O species distinctly decreases, and that of the C=O species slightly decreases with the detection depth in the LiFSI electrolyte (Figure 3a and b). However, the content of nearly all the organic components decreases with the detection depth in the LiPF₆ electrolyte. These demonstrate that the distribution and contents of the organic species in the SEI film are significantly different in these two electrolytes, owing to their different solute anions. This difference should be responsible for the distinct protection effects of the SEI films in these two electrolytes under the lithium plating potential.

The S–F bond (687.5 eV)²² and Li_xPO_yF_z (at 686.8 eV)²⁶ in the F 1s spectrum are derived from LiFSI and LiPF₆, respectively (Figure 3c and d). In addition, LiF (684.2 eV)²⁰ was detected at all the detection depths, and its content was higher in the LiFSI electrolyte than in the LiPF₆ electrolyte. It is interesting that S–F bond was only detected on the SEI surface in the LiFSI electrolyte, while Li_xPO_yF_z was omnipresent throughout the SEI film in the LiPF₆ electrolyte. Figure 3e shows that the content of the F-containing species in the LiPF₆ electrolyte is much higher than that in the LiFSI electrolyte, implying that more PF₆[−] anions are consumed or decomposed during cycling. The S 2p spectra also prove that the content of the FSI[−]-related reduction products is rather lower inside the SEI film than on its surface (Figure S12). The difference in the distribution of the reduction products implies that the SEI film is porous in the LiPF₆ electrolyte but compact in the LiFSI electrolyte. A porous SEI film provides more opportunities for the electrolyte to react with lithium and in turn lowers its protection effect in the LiPF₆ electrolyte. In contrast, the compact SEI film maintains its protection role in the LiFSI electrolyte below 0.0 V. A comparative study indicates that the LiPF₆ electrolyte and/or its derived SEI film are/is more unstable under the lithium deposition potential at the elevated temperature (Figure S13). However, the LiFSI electrolyte and its derived SEI film are less affected with the temperature. Moreover, the shifting of the Li 1s peak may mean that the SEI film is thinner in the LiFSI electrolyte than in the LiPF₆ electrolyte (Figure S14).

The cryo-TEM images of 80 positions on the charged graphite were analyzed to gain further insight into the composition and nanostructure of the SEI film (Figure S15). In accordance with the XPS detection results, the statistics (Figure 3f) indicate that LiF is detected more frequently, while Li₂CO₃ is observed significantly less frequently in the LiFSI electrolyte than in the LiPF₆ electrolyte. The presence of more LiF is known to be critically important in the formation of a uniform and stable SEI film.^{12,27} In addition, cryo-TEM imaging illustrates that the SEI films in both electrolytes have a mosaic structure in which the inorganic species and the organic species are distributed randomly (Figure 3g and h). The nanostructure and composition distribution of the SEI film are usually controlled by the electrolyte solvent, additives, and current density.²⁸ The above results indicate that the lithium salt also has important impacts on the nanostructure and composition distribution of the SEI film.

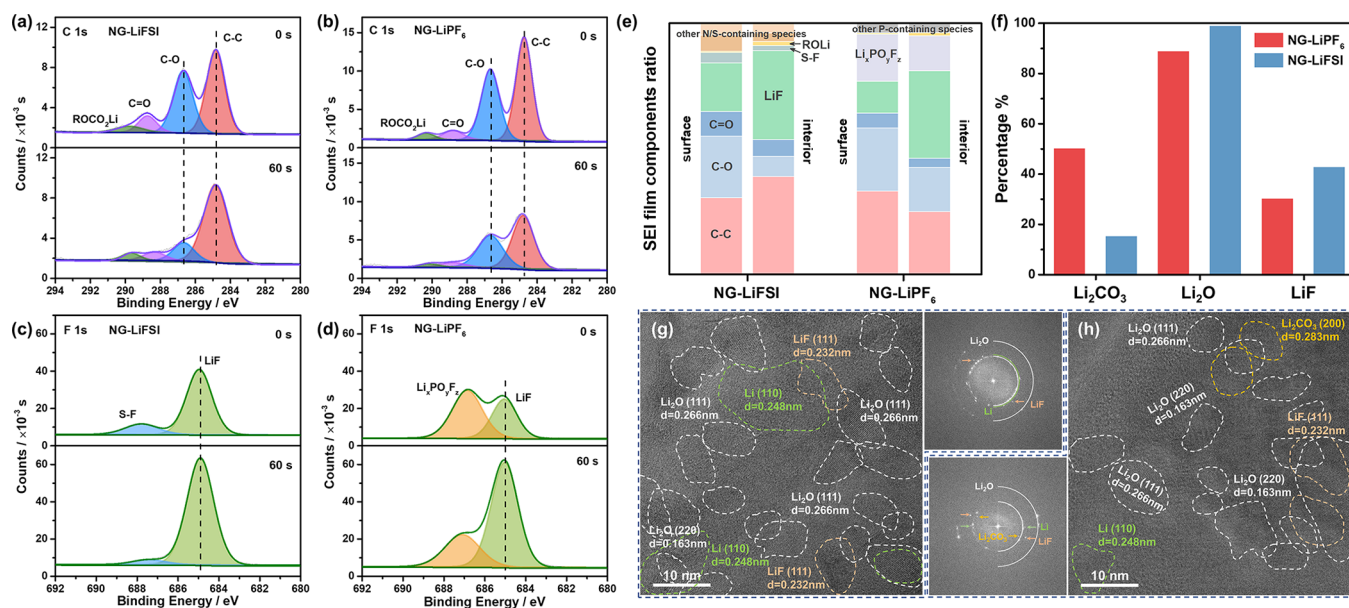


Figure 3. Recognition of the SEI composition on the graphite in the LiFSI and LiPF₆ electrolytes after 20 cycles by (a–e) XPS spectroscopy and (f–h) cryo-TEM imaging. Panel g is for the NG–LiFSI cell, and panel h is for the NG–LiPF₆ cell. (e) Comparison of the SEI composition on the samples in different electrolytes by XPS analysis. (f) Statistics for Li₂CO₃, Li₂O, and LiF in the SEI film detected at different sample positions, that is, the percentages (relative frequencies of being found) of the detected Li₂CO₃, Li₂O, and LiF in different electrolytes.

INTERPHASE EVOLUTION

Although the lithium-ion intercalation/deintercalation cycle well in graphite in these two EC/DMC electrolytes (Figure S16), the lithium plating/stripping cycle on the graphite is significantly dependent on the electrolyte salt (Figure 2). The poor lithium cycling in the LiPF₆ electrolyte should clearly be ascribed to the porous feature of the SEI film and the loss of its protection to graphite under the lithium deposition potential. However, a few authors reported the evolution of the SEI film during lithium plating/stripping. To correlate the property of the SEI film with the lithium cycling performance on graphite, different discharge and charge states in the initial cycle were selected, and the corresponding SEI films were comprehensively characterized (Figure 4).

A comparison of the SEI compositions at different discharge/recharge states indicates that organic species dominate the SEI film at all states in both electrolytes. The intensity of most of the peaks decreases upon lithium plating in the LiPF₆ electrolyte; only the intensity of the peak at 290.3 eV for the carbonate species (ROCOOLi and Li₂CO₃) decreases in the LiFSI electrolyte (Figure 4a and b). These infer the severe decomposition of the SEI film in the LiPF₆ electrolyte and mean that the organic species in the SEI film formed above 0.0 V is unstable against metallic lithium in the LiPF₆ electrolyte; however, the SEI film in the LiFSI electrolyte is more stable.

The weak peak at 285.7 eV for the C–S bond appears on the lithium-covered graphite in the LiFSI electrolyte (Figure 4a). This species, as an intermediate product of the FSI[−] reduction, decomposes after the cell charges to 0.1 V to form other derived species and repair the SEI film. The above inference was proven with the S 2p and N 1s spectra (Figure 4c and d) as the S–F and N–S bonds in FSI[−] are labile to reduction.²⁹ The SEI film at the recharged state (0.1 V) in the first two cycles shares similar compositions (Figure 4a), suggesting the initial formation of a stable SEI film against metallic lithium in the LiFSI electrolyte after the initial cycle. After five cycles, the

CE remains stable, and the charged graphite (0.1 V) has a complete structure and a uniform and compact SEI film in the LiFSI electrolyte (Figure S17a). Although the FSI[−] anion is labile to reduction on the metallic lithium, the stable and compact SEI film in the LiFSI electrolyte can effectively inhibit its further decomposition.³⁰ These suggest that the FSI[−]-derived SEI film remains stable and compact under the lithium deposition potential and effectively protects the graphite and the deposited lithium from continuous reactions with the carbonate electrolyte, thereby boosting the efficiency and cycle stability.²⁰

In contrast, the composition of the SEI film in the LiPF₆ electrolyte keeps changing during lithium plating and stripping (Figure 4b). The structure of the graphite is destroyed as it charges to 0.1 V, and its SEI film becomes inhomogeneous after five cycles (Figure S17b). These mean that this SEI film is unstable against the metallic lithium. In addition, no P 2p signals and a negligible amount of Li_xPO_yF_z were detected inside the SEI film in the initial cycle (Figure 4e and S18, respectively), indicating that the PF₆[−] anions only participate in the formation of LiF in the SEI film. However, plenty of phosphorus-containing species were detected in the aged (20 cycled) SEI film in the LiPF₆ electrolyte (Figure S19). This paradox may mean that these phosphorus-containing species are actually the reaction products from the PF₅ attack against the SEI film and metallic lithium. It was reported that the generation of PF₅ due to PF₆[−] degradation and its leaching effect on the SEI components are responsible for the failure to form a stable SEI film in the lithium-ion battery.^{31,32} However, the situation might be more complicated for the secondary lithium batteries because the degradation of the PF₆[−] anions can become more severe under the lithium plating potential. Therefore, PF₅ can damage the SEI stability by leaching some of its components, resulting in a porous SEI film and deteriorated electrolyte decomposition.³³ This also makes the distribution of the organic composition of the aged SEI film independent of the depth (Figure 3b). Moreover, PF₅

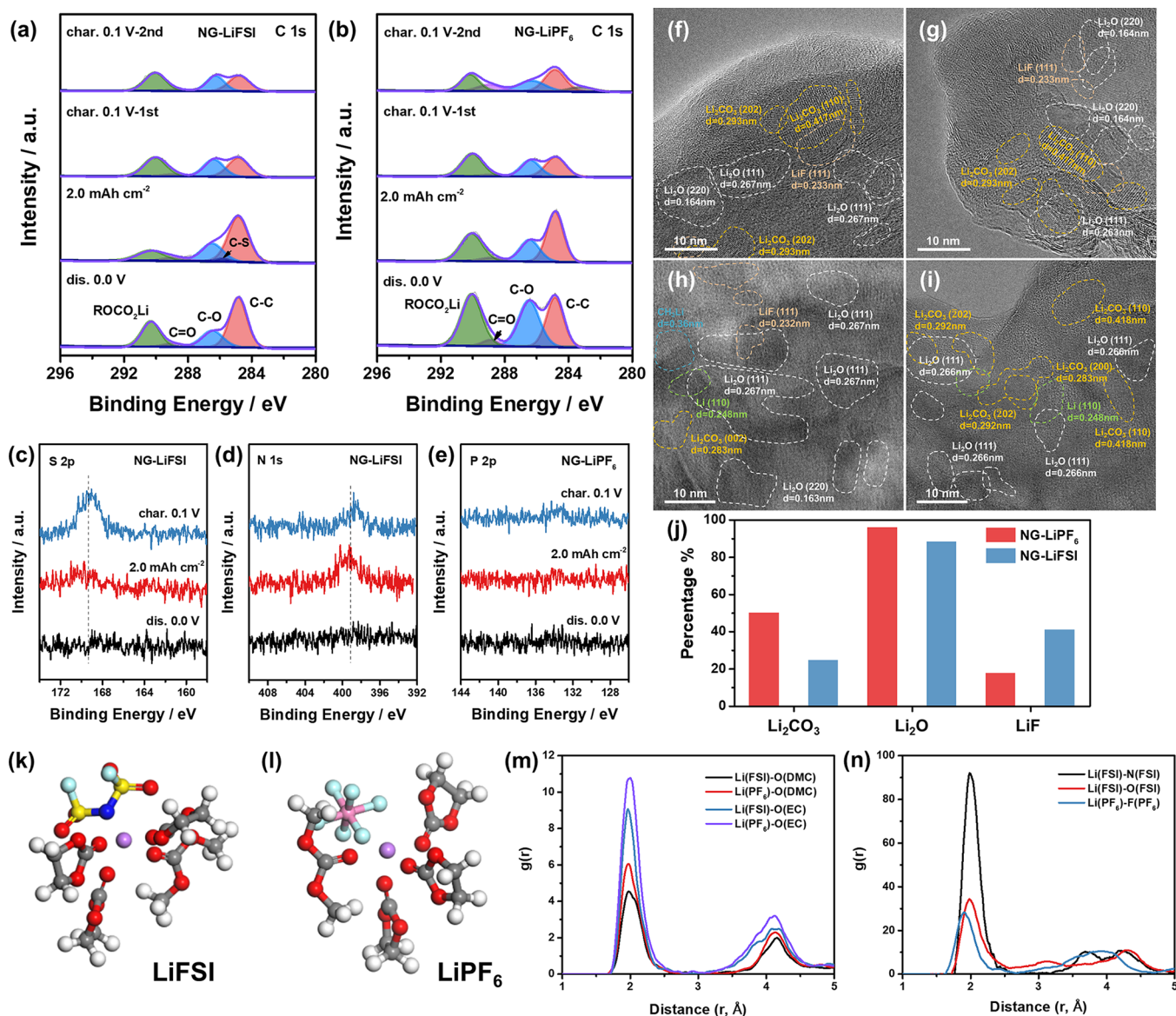


Figure 4. Evolution of the composition and structure of the SEI film in the initial cycle. (a–e) XPS spectra and (f–i) cryo-TEM images. The NG–LiFSI cell was (f) discharged to 0.0 V and (h) charged to 0.1 V, and the NG–LiPF₆ cell was (g) discharged to 0.0 V and (i) charged to 0.1 V. (j) Statistics of the three main inorganic species recognized by cryo-TEM imaging, (k and l) the calculated lithium-ion solvation structures (red balls for O, gray balls for C, white balls for H, purple balls for Li, dark blue balls for N, yellow balls for S, light blue balls for F, and pink balls for P), and (m and n) the radial distribution functions in 1 M LiFSI EC/DMC (1:1) and 1 M LiPF₆ EC/DMC (1:1) electrolytes, respectively.

formation is accelerated in the LiPF₆ electrolyte at high temperatures and promotes the decomposition of the carbonate solvents,³⁴ resulting in poor lithium cycling at the elevated temperatures (Figure S4). However, different from the PF₆⁻ anions, the FSI⁻ anions participate in SEI formation and do not decompose to produce harmful species during lithium plating, ensuring the stability of the SEI film. The impedances of the two cells after the initial lithium plating also clearly shows the stability of the electrode/electrolyte interface in these two electrolytes (Figure S20).

Cryo-TEM imaging shows that the SEI film is mosaic-like in both electrolytes. It contains LiF and some amorphous species, but Li₂CO₃ and Li₂O are the dominating inorganic species before lithium plating (Figure 4f and g). The Li₂CO₃ content decreases, and Li₂O becomes the main inorganic species in the SEI film after one lithium plating/stripping cycle (Figure 4h–i). In addition, “dead” lithium was observed in the SEI film in

both electrolytes, implying that the formation of the “dead” lithium is also responsible for the low initial Coulombic efficiency. The statistical analysis of the compositions of more than 30 different positions of the SEI film (Figure S21) indicates that the LiF content is obviously higher in the LiFSI electrolyte than in the LiPF₆ electrolyte (Figure 4j), meaning that the FSI⁻ anions are more labile to participate in the formation of the SEI film during lithium plating. These findings suggest that the compact SEI film contains more LiF as a reduction product of the FSI⁻ anions, but that by the PF₆⁻ reduction does not.

The SEI composition is closely related to the solvation structure of the electrolyte and the selective reduction of the electrolyte components on the anode. Molecular dynamics (MD) simulations were performed to further understand the impacts of the FSI⁻ anions on the composition of the SEI film (Figure 4k–l). The peaks at around 1.97, 1.90, and 1.98 Å in

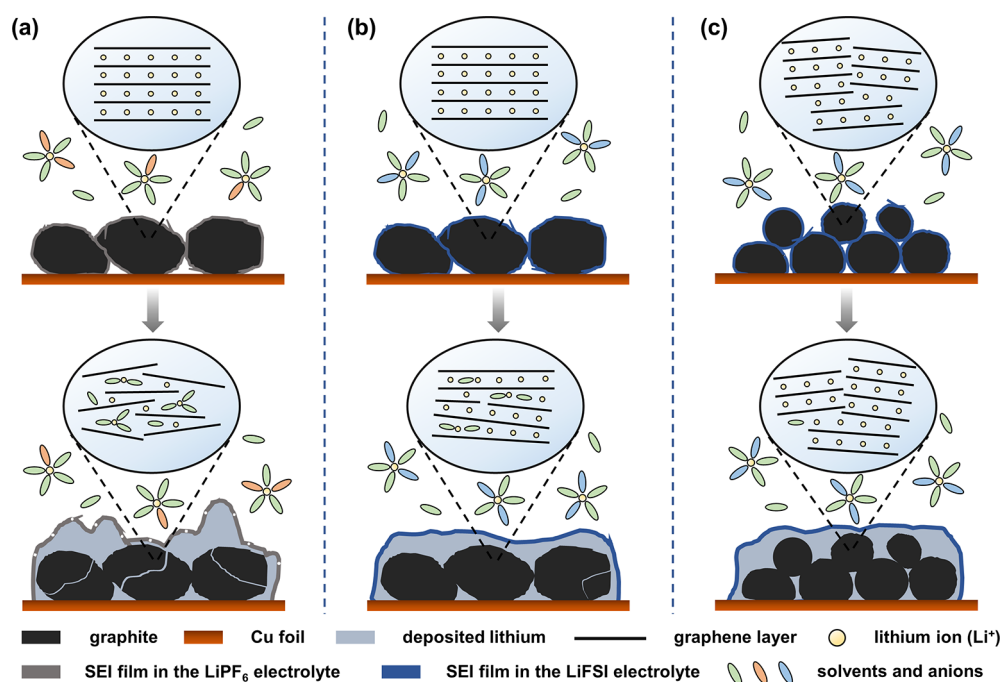


Figure 5. Schematic illustration of the effect of the anion in the electrolyte and the particle size of graphite on both the evolution of the graphite structure and lithium deposition for (a) the NG-LiPF₆ cell, (b) the NG-LiFSI cell, and (c) the BMG-LiFSI cell.

the radial distribution function (RDF) are for the distance of the Li⁺-carbonate solvents, i.e., Li⁺-F(PF₆⁻) and Li⁺-N/O(FSI⁻), respectively (Figure 4m and n), indicating that the PF₆⁻ or FSI⁻ anion is within the first solvation shell and exists in the form of contact ion pairs (CIP). The calculated Li⁺-anion coordination numbers are 1.8 and 2.0 in the LiPF₆ and LiFSI electrolytes, respectively. Such a configuration is commonly associated with highly desirable properties, including a high Li⁺ transference number and improved electrochemical stability.^{17,20} This also means that more FSI⁻ anions are contained in a Li⁺-solvent or Li⁺-anion solvation shell than the PF₆⁻ anions are. In addition, ion-paired LiPF₆ is prone to dissociation into PF₅, which can attack the SEI film and the metallic lithium.³² Therefore, it is understandable that more FSI⁻ anions are reduced and contribute to the formation of LiF and other species as the solvated lithium ions diffuse to the anode surface, leading to a compact SEI film rich in LiF but lean in carbonate derivatives.²²

The above results and discussions indicate that a stable and compact SEI film is formed in the LiFSI electrolyte, and this electrolyte is beneficial for enhancing the lithium utilization and protecting the integration of the graphite structure. Reducing the graphite particle size can further alleviate the particle pulverization, thereby increasing the Coulombic efficiency and cycle lifespan.⁹ Figure 5 schematically summarizes the effects of the lithium salt and the graphitic particle size on the evolution of the carbon structure and the morphology of the deposited lithium.

In summary, the application of LiFSI as the electrolyte salt in the carbonate electrolyte enhances the cycling performance of lithium deposition on the graphite substrate. The FSI⁻ anion was found to be responsible for the stability of the compact SEI film and the protection of the graphite structure that is vulnerable to the deposited lithium. More FSI⁻ anions are contained in a Li⁺ solvation shell in the LiFSI electrolyte than in the LiPF₆ electrolyte and can participate in the formation of

the compact and stable SEI film during lithium plating. The FSI⁻-derived SEI film protects the graphite substrate from the co-intercalation of the solvated lithium ions and suppresses the continuous reaction between the electrolyte and the deposited lithium, prolonging the lifespan of the cell and enhancing its Coulombic efficiencies. These findings renew the understanding of the stability of the SEI film and provide a suggestion on the design and development of electrolytes for secondary lithium batteries.

■ ASSOCIATED CONTENT

Supporting Information

The Supporting Information is available free of charge at <https://pubs.acs.org/doi/10.1021/acs.nanolett.1c01436>.

Details on experimental methods; XRD, EIS, Raman, FTIR, and XPS spectra; SEM and TEM images; and electrochemical performance details (PDF)

■ AUTHOR INFORMATION

Corresponding Authors

Xuefeng Wang – School of Physical Sciences and College of Materials Science and Opto-Electronic Technology, University of Chinese Academy of Sciences, Beijing 100190, China; Laboratory for Advanced Materials and Electron Microscopy, Institute of Physics, Chinese Academy of Sciences, Beijing 100190, China; Tianmu Lake Institute of Advanced Energy Storage Technologies Co. Ltd., Liyang 213300, Jiangsu, China; orcid.org/0000-0001-9666-8942; Email: wxf@iphy.ac.cn

Zhaoxiang Wang – Key Laboratory for Renewable Energy, Beijing Key Laboratory for New Energy Materials and Devices, Institute of Physics, Chinese Academy of Sciences, Beijing 100190, China; School of Physical Sciences and College of Materials Science and Opto-Electronic Technology, University of Chinese Academy of Sciences, Beijing 100190,

China; orcid.org/0000-0002-1123-6591;
Email: zxwang@iphys.ac.cn

Authors

Gaojing Yang – Key Laboratory for Renewable Energy, Beijing Key Laboratory for New Energy Materials and Devices, Institute of Physics, Chinese Academy of Sciences, Beijing 100190, China; School of Physical Sciences, University of Chinese Academy of Sciences, Beijing 100190, China; orcid.org/0000-0002-9275-316X

Simeng Zhang – Key Laboratory for Renewable Energy, Beijing Key Laboratory for New Energy Materials and Devices, Institute of Physics, Chinese Academy of Sciences, Beijing 100190, China; College of Materials Science and Opto-Electronic Technology, University of Chinese Academy of Sciences, Beijing 100190, China

Suting Weng – School of Physical Sciences, University of Chinese Academy of Sciences, Beijing 100190, China; Laboratory for Advanced Materials and Electron Microscopy, Institute of Physics, Chinese Academy of Sciences, Beijing 100190, China

Xiaoyun Li – Key Laboratory for Renewable Energy, Beijing Key Laboratory for New Energy Materials and Devices, Institute of Physics, Chinese Academy of Sciences, Beijing 100190, China; College of Materials Science and Opto-Electronic Technology, University of Chinese Academy of Sciences, Beijing 100190, China

Liquan Chen – Key Laboratory for Renewable Energy, Beijing Key Laboratory for New Energy Materials and Devices, Institute of Physics, Chinese Academy of Sciences, Beijing 100190, China; School of Physical Sciences and College of Materials Science and Opto-Electronic Technology, University of Chinese Academy of Sciences, Beijing 100190, China

Complete contact information is available at:

<https://pubs.acs.org/10.1021/acs.nanolett.1c01436>

Notes

The authors declare no competing financial interest.

ACKNOWLEDGMENTS

We appreciated the help of Prof. Feng Wu and Prof. Renjie Chen at the Beijing Institute of Technology with the molecular dynamics simulations in this work. This work was financially supported by the National Natural Science Foundation of China (NSFC 21773301 and 22005334) and the Natural Science Foundation of Beijing (Grant Z200013).

REFERENCES

- (1) Zhang, X.; Yang, Y.; Zhou, Z. Towards practical lithium-metal anodes. *Chem. Soc. Rev.* **2020**, *49* (10), 3040–3071.
- (2) Zuo, T.-T.; Wu, X.-W.; Yang, C.-P.; Yin, Y.-X.; Ye, H.; Li, N.-W.; Guo, Y.-G. Graphitized Carbon Fibers as Multifunctional 3D Current Collectors for High Areal Capacity Li Anodes. *Adv. Mater.* **2017**, *29* (29), 1700389.
- (3) Li, X.; Yang, G.; Zhang, S.; Wang, Z.; Chen, L. Improved lithium deposition on silver plated carbon fiber paper. *Nano Energy* **2019**, *66*, 104144.
- (4) Sun, Y.; Zheng, G.; Seh, Z. W.; Liu, N.; Wang, S.; Sun, J.; Lee, H. R.; Cui, Y. Graphite-Encapsulated Li-Metal Hybrid Anodes for High-Capacity Li Batteries. *Chem.* **2016**, *1* (2), 287–297.
- (5) Ye, H.; Xin, S.; Yin, Y.-X.; Li, J.-Y.; Guo, Y.-G.; Wan, L.-J. Stable Li Plating/Stripping Electrochemistry Realized by a Hybrid Li Reservoir in Spherical Carbon Granules with 3D Conducting Skeletons. *J. Am. Chem. Soc.* **2017**, *139* (16), 5916–5922.

(6) Martin, C.; Genovese, M.; Louli, A. J.; Weber, R.; Dahn, J. R. Cycling Lithium Metal on Graphite to Form Hybrid Lithium-Ion/Lithium Metal Cells. *Joule* **2020**, *4* (6), 1296–1310.

(7) Kaskhedikar, N. A.; Maier, J. Lithium Storage in Carbon Nanostructures. *Adv. Mater.* **2009**, *21* (25–26), 2664–2680.

(8) Cabañero, M. A.; Hagen, M.; Quiroga-González, E. In-operando Raman study of lithium plating on graphite electrodes of lithium ion batteries. *Electrochim. Acta* **2021**, *374*, 137487.

(9) Yang, G.; Zhang, S.; Tong, Y.; Li, X.; Wang, Z.; Chen, L. Minimizing carbon particle size to improve lithium deposition on natural graphite. *Carbon* **2019**, *155*, 9–15.

(10) Yang, G.; Li, Y.; Tong, Y.; Qiu, J.; Liu, S.; Zhang, S.; Guan, Z.; Xu, B.; Wang, Z.; Chen, L. Lithium Plating and Stripping on Carbon Nanotube Sponge. *Nano Lett.* **2019**, *19* (1), 494–499.

(11) Xu, W.; Wang, J.; Ding, F.; Chen, X.; Nasybulin, E.; Zhang, Y.; Zhang, J.-G. Lithium metal anodes for rechargeable batteries. *Energy Environ. Sci.* **2014**, *7* (2), 513–537.

(12) Zhang, X.-Q.; Cheng, X.-B.; Chen, X.; Yan, C.; Zhang, Q. Fluoroethylene Carbonate Additives to Render Uniform Li Deposits in Lithium Metal Batteries. *Adv. Funct. Mater.* **2017**, *27* (10), 1605989.

(13) Markevich, E.; Salitra, G.; Chesneau, F.; Schmidt, M.; Aurbach, D. Very Stable Lithium Metal Stripping-Plating at a High Rate and High Areal Capacity in Fluoroethylene Carbonate-Based Organic Electrolyte Solution. *ACS Energy Lett.* **2017**, *2* (6), 1321–1326.

(14) Xiang, H.; Shi, P.; Bhattacharya, P.; Chen, X.; Mei, D.; Bowden, M. E.; Zheng, J.; Zhang, J.-G.; Xu, W. Enhanced charging capability of lithium metal batteries based on lithium bis-(trifluoromethanesulfonyl)imide-lithium bis(oxalato)borate dual-salt electrolytes. *J. Power Sources* **2016**, *318*, 170–177.

(15) Zheng, J.; Engelhard, M. H.; Mei, D.; Jiao, S.; Polzin, B. J.; Zhang, J.-G.; Xu, W. Electrolyte additive enabled fast charging and stable cycling lithium metal batteries. *Nature Energy* **2017**, *2*, 17012.

(16) Suo, L.; Xue, W.; Gobet, M.; Greenbaum, S. G.; Wang, C.; Chen, Y.; Yang, W.; Li, Y.; Li, J. Fluorine-donating electrolytes enable highly reversible 5-V-class Li metal batteries. *Proc. Natl. Acad. Sci. U. S. A.* **2018**, *115* (6), 1156–1161.

(17) Holoubek, J.; Yu, M.; Yu, S.; Li, M.; Wu, Z.; Xia, D.; Bhaladhare, P.; Gonzalez, M. S.; Pascal, T. A.; Liu, P.; Chen, Z. An All-Fluorinated Ester Electrolyte for Stable High-Voltage Li Metal Batteries Capable of Ultra-Low-Temperature Operation. *ACS Energy Lett.* **2020**, *5* (5), 1438–1447.

(18) Ding, F.; Xu, W.; Chen, X.; Zhang, J.; Engelhard, M. H.; Zhang, Y.; Johnson, B. R.; Crum, J. V.; Blake, T. A.; Liu, X.; Zhang, J.-G. Effects of Carbonate Solvents and Lithium Salts on Morphology and Coulombic Efficiency of Lithium Electrode. *J. Electrochem. Soc.* **2013**, *160* (10), A1894–A1901.

(19) Han, H.-B.; Zhou, S.-S.; Zhang, D.-J.; Feng, S.-W.; Li, L.-F.; Liu, K.; Feng, W.-F.; Nie, J.; Li, H.; Huang, X.-J.; Armand, M.; Zhou, Z.-B. Lithium bis(fluorosulfonyl)imide (LiFSI) as conducting salt for nonaqueous liquid electrolytes for lithium-ion batteries: Physico-chemical and electrochemical properties. *J. Power Sources* **2011**, *196* (7), 3623–3632.

(20) Chen, S.; Zheng, J.; Mei, D.; Han, K. S.; Engelhard, M. H.; Zhao, W.; Xu, W.; Liu, J.; Zhang, J. G. High-Voltage Lithium-Metal Batteries Enabled by Localized High-Concentration Electrolytes. *Adv. Mater.* **2018**, *30* (21), 1706102.

(21) Fan, X.; Chen, L.; Ji, X.; Deng, T.; Hou, S.; Chen, J.; Zheng, J.; Wang, F.; Jiang, J.; Xu, K.; Wang, C. Highly Fluorinated Interphases Enable High-Voltage Li-Metal Batteries. *Chem.* **2018**, *4* (1), 174–185.

(22) Yang, G.; Li, Y.; Liu, S.; Zhang, S.; Wang, Z.; Chen, L. LiFSI to improve lithium deposition in carbonate electrolyte. *Energy Storage Mater.* **2019**, *23*, 350–357.

(23) Xue, W.; Shi, Z.; Huang, M.; Feng, S.; Wang, C.; Wang, F.; Lopez, J.; Qiao, B.; Xu, G.; Zhang, W.; Dong, Y.; Gao, R.; Shao-Horn, Y.; Johnson, J. A.; Li, J. FSI-inspired solvent and “full fluorosulfonyl” electrolyte for 4 V class lithium-metal batteries. *Energy Environ. Sci.* **2020**, *13* (1), 212–220.

- (24) Zhang, S.; Yang, G.; Liu, S.; Li, X.; Wang, X.; Wang, Z.; Chen, L. Understanding the Dropping of Lithium Plating Potential in Carbonate Electrolyte. *Nano Energy* **2020**, *70*, 104486.
- (25) Mogi, R.; Inaba, M.; Jeong, S.-K.; Iriyama, Y.; Abe, T.; Ogumi, Z. Effects of Some Organic Additives on Lithium Deposition in Propylene Carbonate. *J. Electrochem. Soc.* **2002**, *149* (12), A1578.
- (26) Wang, X.; Zhang, M.; Alvarado, J.; Wang, S.; Sina, M.; Lu, B.; Bouwer, J.; Xu, W.; Xiao, J.; Zhang, J.-G.; Liu, J.; Meng, Y. S. New Insights on the Structure of Electrochemically Deposited Lithium Metal and Its Solid Electrolyte Interphases via Cryogenic TEM. *Nano Lett.* **2017**, *17* (12), 7606–7612.
- (27) Lu, Y.; Tu, Z.; Archer, L. A. Stable lithium electrodeposition in liquid and nanoporous solid electrolytes. *Nat. Mater.* **2014**, *13* (10), 961–969.
- (28) Xu, Y.; Wu, H.; He, Y.; Chen, Q.; Zhang, J.-G.; Xu, W.; Wang, C. Atomic to Nanoscale Origin of Vinylene Carbonate Enhanced Cycling Stability of Lithium Metal Anode Revealed by Cryo-Transmission Electron Microscopy. *Nano Lett.* **2020**, *20* (1), 418–425.
- (29) Li, X.; Zheng, J.; Engelhard, M. H.; Mei, D.; Li, Q.; Jiao, S.; Liu, N.; Zhao, W.; Zhang, J.-G.; Xu, W. Effects of Imide-Orthoborate Dual-Salt Mixtures in Organic Carbonate Electrolytes on the Stability of Lithium Metal Batteries. *ACS Appl. Mater. Interfaces* **2018**, *10* (3), 2469–2479.
- (30) Zheng, H.; Xiang, H.; Jiang, F.; Liu, Y.; Sun, Y.; Liang, X.; Feng, Y.; Yu, Y. Lithium Difluorophosphate-Based Dual-Salt Low Concentration Electrolytes for Lithium Metal Batteries. *Adv. Energy Mater.* **2020**, *10* (30), 2001440.
- (31) Campion, C. L.; Li, W.; Lucht, B. L. Thermal Decomposition of LiPF₆-Based Electrolytes for Lithium-Ion Batteries. *J. Electrochem. Soc.* **2005**, *152* (12), A2327.
- (32) Han, J.-G.; Kim, K.; Lee, Y.; Choi, N.-S. Scavenging Materials to Stabilize LiPF₆-Containing Carbonate-Based Electrolytes for Li-Ion Batteries. *Adv. Mater.* **2019**, *31* (20), 1804822.
- (33) Zhang, S.; Yang, G.; Liu, Z.; Li, X.; Wang, X.; Chen, R.; Wu, F.; Wang, Z.; Chen, L. Competitive Solvation Enhanced Stability of Lithium Metal Anode in Dual-Salt Electrolyte. *Nano Lett.* **2021**, *21* (7), 3310–3317.
- (34) Sloop, S. E.; Pugh, J. K.; Wang, S.; Kerr, J. B.; Kinoshita, K. Chemical Reactivity of PF₅ and LiPF₆ in Ethylene Carbonate/Dimethyl Carbonate Solutions. *Electrochem. Solid-State Lett.* **2001**, *4* (4), A42.